

Fast and Slow Sound Excitations in Nematic Aerogel in superfluid ^3He

A.M. Bratkovsky

*Kapitza Institute for Physical Problems, Moscow 119334, Russia**

(Dated: March 12, 2026)

Nematic aerogel (nAG) supports so-called polar phase in liquid ^3He . The experiments [Dmitriev *et al.*, JETP Lett. **112**, 780 (2020)] showed that the onset of polar phase inside the nAG is accompanied by emergence of a sound wave with frequency quickly growing with cooling down from transition temperature and reaching a plateau. To describe this behavior, we start by calculating the elastic properties of the dry nematic AG that appear to depend only on Young's modulus of the parent material (e.g. mullite), the volume fraction of the solid phase ψ ($= 5\%$) and the aspect ratio of the representative volume of nAG. The elastic constants are then used to solve elasto-hydrodynamic equations for various sound vibrations of nAG filled with ^3He . The (isotropic) first sound and anisotropic second sound in the polar phase are strongly hybridized with fourth sound and standard elastic modes in nAG. The hybrid second and the transverse fourth sound start with zero velocity at the transition, similar to pure ^3He , and quickly grow with lowering temperature until they hit the sample finite size cutoff.

PACS numbers: 67.30.ef, 67.30.hm, 67.30.hj, 43.35.Mr, 62.20.de

I. INTRODUCTION

Helium three, ^3He , is the only topological superfluid accessible in laboratory conditions. It is intrinsically anisotropic sharing some features with liquid crystals[1]. The polar phase of superfluid ^3He , that was expected for quite a while to be stabilized in anisotropic aerogel[2], was found and studied extensively since 2015[3–5]. Very strong anisotropy of filamentary porous media housing ^3He is required, and it was provided by new type of nematic aerogel (nAG). The signatures of the polar phase have been found in experiments where nAG was attached to a *vibrating wire* (VW.) This technique has been used extensively to study ^3He , see review [6]. In addition to finding the polar phase, Dmitriev *et al.* have found the so-called *beta-phase* of ^3He in magnetic field [7]. Both polar- and beta-phases are equal spin pairing (ESP) so that the condensate of the Cooper pairs is made of aligned spin pairs like $|\uparrow\uparrow\rangle$. Wave function of the pair in momentum k -space is the 2×2 bispinor $\Psi_{\sigma\sigma'}(\hat{\mathbf{k}})$ ($\hat{\mathbf{k}}$ is the unit k -vector), σ, σ' the spin quantum numbers of ^3He atoms in the pair). One may construct a vector $d_\lambda(\hat{\mathbf{k}}) = -i \text{tr}(\Psi_{\sigma\sigma'}\sigma_2\sigma_\lambda) \equiv A_{\lambda j}\hat{k}_j$, with d_λ living in spin space, $\sigma_\lambda = (\sigma_1, \sigma_2, \sigma_3)$ the vector of Pauli matrices. Its k -dependence must be linear for p-wave orbital state of the pair, $L = 1$, and this explains the last equality. The matrix $A_{\lambda j}$ (the order parameter) defines the properties of particular phases that are formed at a certain pressure, boundary conditions, and internal perturbations like interactions with embedded aerogel. The so-called B-phase has the simplest structure, $d_\lambda(\hat{\mathbf{k}}) \propto \hat{\mathbf{k}}$, with isotropic gap in spectrum of Bogoliubov quasiparticles, $\Delta_{\mathbf{k}} \propto |d_\lambda(\hat{\mathbf{k}})|^2 = \text{const}$. The ^3He interactions with embedded *nematic* aerogel favor

'uniaxial' $d_\lambda(\hat{\mathbf{k}}) \propto \hat{k}_z = \cos\theta$, where θ the polar angle with the *director* of the nematic aerogel \mathbf{m} that we select as the z -axis. This yields the gap $\Delta_{\mathbf{k}} \propto \hat{k}_z^2 = \cos^2\theta$ with the Dirac nodal line along the equator of the fermi surface, $\theta = \pi/2$. The spin *projection* of the Cooper pair along z -axis vanishes, $S_z = 0$ (total spin of the pair is $S = 1$) since its wave function is $\Psi_{\text{pair}}^{\text{polar}} \propto \hat{k}_z(|\uparrow\uparrow\rangle + |\downarrow\downarrow\rangle)$ for $\mathbf{d} \propto (0, -ik_z, 0)$ using z -axis quantization. In variance with the *polar* phase, its sibling the *beta* phase only comprises a pair of up-spins $|\uparrow\uparrow\rangle$ and no down-spins in external magnetic field, with $\mathbf{d} \propto (-k_z, -ik_z, 0)$, thus making it similar to A_1 phase. The β phase also has a gap with a nodal line running along equator of fermi surface. The strongly anisotropic nematic AG orients the Cooper pairs so that the superfluid phase has maximal value of the gap at the $\pm\hat{z}$ poles, where \hat{z} is the unit vector pointing along the growth direction (parallel to the director \mathbf{m}).

Both polar- and beta-phases of ^3He have been discovered using approximately $(3 \text{ mm})^3$ nematic AG glued to an apex of an arch-shaped vibrating wire (VW) subject to the driving AC current in external magnetic field. The sample oscillated along the strands. The strands have diameters about 14 nm and average separation between them about 60 nm (the volume fraction of the solid part $\psi \approx 5\%$.) The observed frequency range has been $f = 500 - 1600$ Hz. Importantly, the viscous penetration depth $\delta \approx 0.3$ mm was much larger than the spacing between the strands even near T_c at $P = 29.3$ bar [5] meaning that the *normal component* in the above experiment is always *clamped to the aerogel*. Since nAG drags along the normal part, the overall dynamics of vibrations changes drastically especially because the density of superfluid motion parallel to the strands is at least three times that perpendicular to the strands, $\rho_{\parallel}^s/\rho_{\perp}^s \geq 3$, near critical temperature of interest to us (the lower limit corresponds to a weak coupling approximation.) Thus, the effective mass density involved in various sound vi-

* alex.bratkovski@gmail.com

brations of the combined system ^3He -nAG depends on the polarization of those vibrations. This should be contrasted with ^4He [8] and ^3He [9] in *isotropic* silica aerogel.

In experiments by Dmitriev *et al.* [5], the vibrating wire with attached nAG has exhibited the main resonance in the normal phase above T_c . Then a rapid decrease of the width has been observed indicating a superfluid transition in bulk ^3He at $T = T_c$. On further cooling, the second resonance has appeared due to the superfluid transition of ^3He into the polar phase in the oscillating sample at $T_{ca} \approx 0.989T_c$. Although the authors have not been able to observe a clear resonance peak at frequencies lower than 470 Hz, they assumed that on cooling from $T = T_{ca}$ the frequency of the second mode rapidly grows from 0 to about 1600 Hz [5].

As far as the origin of observed *additional resonance*, the authors have speculated that the 'slow mode' should correspond to some soft deformations of nAG perpendicular to strands since the sample is very stiff along the strands. This is correct and, in fact, *any* sound but the *longitudinal* fourth sound is slow, as we calculate below without any fitting parameters for all vibrational modes of combined ^3He -nAG system. In fact, the nAG itself supports plenty of slow modes being highly anisotropic extremely porous material with tiny solid state volume fraction $\psi = 5\%$. Without solving for the elastic properties of nematic aerogel first, one is left with large number of unknown fitting parameters to describe the dynamics of anisotropic superfluid encased in highly anisotropic medium, see prior works [10, 11]. Below, we shall calculate all the elastic constants of nAG first and then solve the combined elasto-hydrodynamic equations of motion for all hybrid vibrational modes and give results for the polar phase for sound waves propagating along and perpendicular to the strands. We shall focus on properties of uniform ^3He -nAG and discuss how the finite size of a nAG sample affects the results.

We shall see below that the sample supports many *slow modes* due to elastic vibrations of the AG skeleton that drags along the highly anisotropic normal part of the polar ^3He . They exist above and below transition and weakly depend on temperature with velocities $U \sim 1 - 10$ m/s. Below transition, there appear the *second and fourth sound modes* hybridized with aerogel skeleton vibrations. The hybrid second sounds start with *zero velocity*, $U_{2a}(T_{ca}) = 0$ that increases rapidly with lowering T . The *hybrid fourth sound* has zero velocity at T_{ca} *only* for transversal modes propagating *perpendicular* to the strands, while the hybrid longitudinal fourth sound would have finite and large velocity on the order of $u_1 \gtrsim 100$ m/s at all temperatures, including T_{ca} . This mode is too fast to be excited in small aerogel sample with linear size $L \ll \lambda/2$ (half wavelength of the sound wave) and, therefore, is not responsible for the observed resonances [3, 6]. All modes are described by simple quadratic equations with parameters depending on the propagation direction and polarization of the waves reflecting the anisotropy of both the polar phase of ^3He and

nAG defining the anisotropic hybrid second and fourth sounds. The above simple scenario for 'slow mode' resonance is different from the interesting one studied in Ref.[11] that considered volume-conserving shape oscillations of finite AG sample coupled to a soft mode related to chemical potential coupling to an axial strain. In the present model, the oscillations of the chemical potential are accounted for in a usual way through oscillations of pressure and temperature (two leading terms) in the sound waves[13] and the sound velocities are given as solutions of simple quadratic equation with no singular denominators.

II. ELASTIC PROPERTIES OF NEMATIC AEROGEL

The nematic AG consists of rigid polycrystalline strands of mullite or other inorganic material like Al_2O_3 or $\text{Al}_2\text{O}_3\text{-ZrO}_2$. It is a high-porosity anisotropic network structure that is stiff along the growth z -direction and is elastically isotropic in plane perpendicular to the strands. It would then be characterized by five elastic constants like any transversely isotropic system. The nematic aerogel contains rather straight strands with small waviness along the growth direction, Fig.1(b). They touch along z -axis to form an elastic skeleton with typical separation between the rigid joints c that is much larger than the typical spacing between the strands $a \sim 60$ nm, i.e. $c/a \gg 1$. The typical diameter of the strands is $2r \leq 14$ nm. Our estimates below show that the effective elastic constants of nAG depend only on the Young's modulus of the strands' material E , the aspect ratio c/a , and the solid fraction ψ (about 5% in mullite nAG[5].) Thus, it appears that the present expressions for the elastic constants of nematic AG are rather general. This is in the same vein as the elastic properties of highly porous cellular materials that follow simple scaling laws[14].

To find the effective elastic constants, consider the simplest representative periodic orthorhombic unit cell of AG viewed as an elastic *frame* in Fig. 1 with sides $a \approx b \ll c$. We assume that the strands are rigidly joined at the nodes in accord with TEM data ensuring bending moment continuity. The periodic model is then subjected to uniform strain with strain tensor $e_{ij} = \{e_{xx}, e_{yy}, e_{zz}, e_{yz}, e_{xz}, e_{xy}\}$ or, equivalently, $\{e_1, e_2, e_3, e_4, e_5, e_6\}$ in Voigt notations. The strands will exhibit axial and shear (bending) deformations. One calculates the total energy of the deformed unit cell and equates it to the elastic energy $W_{el} = \frac{1}{2}v_c C_{ijkl} e_{ij} e_{lm}$ [J] through the elastic constants tensor C_{ijkl} [J/m³] and determines all its components in the linear elastic approximation (v_c [m³] is the unit cell volume). We assume Einstein summation rule over repeated indices. This will suffice to study the sound excitations that we are focusing on. Other e.g. *flexural* modes of the strands with $\omega \propto k^2$ dispersion could be accounted for when needed.

For axial strain along z -direction involving c -strands

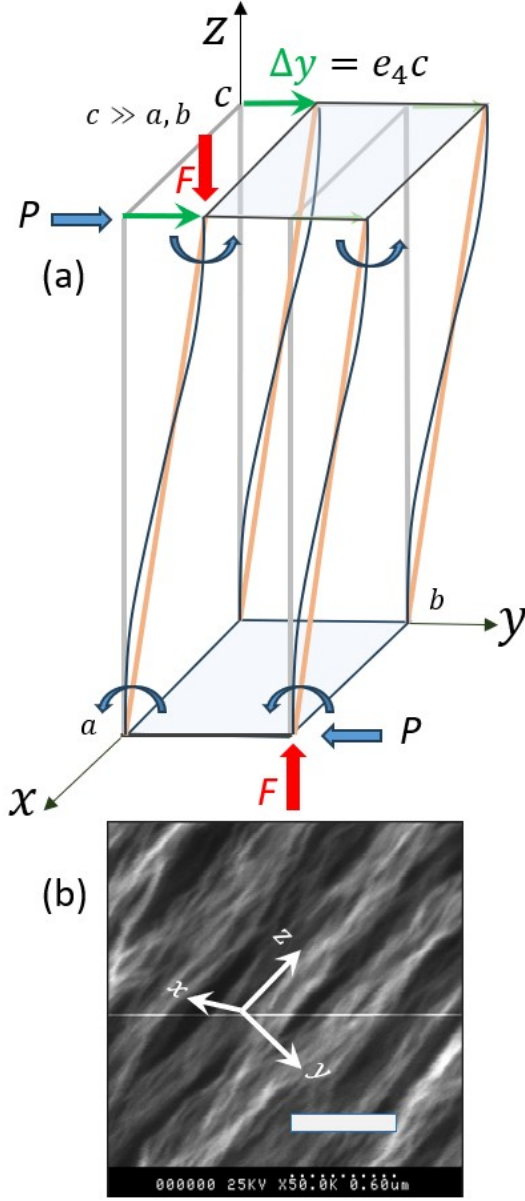


FIG. 1. (Color online) (a) Representative volume of nematic aerogel used to estimate its elastic constants viewed as an equivalent orthorhombic cell with fused nodes. The strands are fused together over the typical distance $c \gg a, b$, where the parameters a and b are typical separation between the strands (~ 60 nm in Ref. [5].) P and F mark the shear and the axial forces resulting in shear strain $e_{23} \equiv e_5$ and axial strain (not shown). Under the load, the fused strands bend and rotate about the nodes. The resulting bending torques on the strands (elastic Euler-Bernoulli "beams") are shown by curved arrows. (b) The STEM picture of nematic aerogel (courtesy V.V. Dmitriev, A.A.Soldatov, and A.N. Yudin.) The size bar is $0.6 \mu\text{m}$.

(Fig.1), the latter will deform by $\delta = e_3c$ with corresponding energy

$$W_{axial}(e_{zz}) = \frac{1}{2}EAc \left(\frac{\delta}{c}\right)^2 = \frac{1}{2}EAc e_3^2, \quad (1)$$

where E is the Young's modulus of the strand material ($E = 150$ GPa for mullite) and $A = \pi r^2$ the cross sectional area of the strand. Analogous results hold for strains along a - and b -strands.

The strains $e_{4\div 6}$ result in bending of the strands and rigid rotations of the nodes (Fig.1). Consider $e_4 \equiv e_{yz}$: the top of the unit cell would shift by $\Delta y = e_{yz}c \equiv e_4c$. The force resulting in this deformation is $P = 12EI \Delta y/c^3$, $I = \pi r^4/4$ [12]. The corresponding energy is

$$W_{bend}(e_{yz}) = \frac{1}{2}P \Delta y = 6EI \frac{e_4^2}{c}. \quad (2)$$

The total elastic energy

$$\begin{aligned} W_{tot} &= \frac{1}{2}v_c c_{\alpha\beta} e_\alpha e_\beta \\ &= \frac{1}{2}EA (ae_1^2 + be_2^2 + ce_3^2) \\ &\quad + 6EI \left[\left(\frac{1}{b} + \frac{1}{c}\right) e_4^2 + \left(\frac{1}{a} + \frac{1}{c}\right) e_5^2 + \left(\frac{1}{a} + \frac{1}{b}\right) e_6^2 \right], \end{aligned} \quad (3)$$

where $v_c = abc$ is the unit cell volume, $\alpha, \beta = 1 \div 6$ are the Voigt indices. This yields the elastic constants

$$\begin{aligned} c_{11}(c_{22}, c_{33}) &= EAa(b, c)/v_c, \\ c_{44} &= 6EI \left(\frac{1}{b} + \frac{1}{c}\right) /v_c, \\ c_{55} &= 6EI \left(\frac{1}{a} + \frac{1}{c}\right) /v_c, \\ c_{66} &= 6EI \left(\frac{1}{a} + \frac{1}{b}\right) /v_c, \end{aligned} \quad (4)$$

with other ones being negligible, meaning that the Poisson coefficients of the aerogel network structure are close to zero. Using the small parameter $a/c \approx b/c \ll 1$, one obtains the important expressions for the 'axial' elastic constants,

$$\begin{aligned} c_{33} &\approx E\psi, \\ c_{11} \approx c_{22} &\approx E\psi \frac{a}{c} \ll c_{33}, \end{aligned} \quad (5)$$

and for the shear constants,

$$c_{44} \approx \frac{3}{2\pi} E\psi^2 \frac{a}{c}, \quad c_{55} \approx c_{44}, \quad c_{66} \sim 2c_{44}, \quad (6)$$

$$c_{44,55,66} \ll c_{11,22} \ll c_{33}. \quad (7)$$

The shear constants contain an extra factor ψ , the small volume fraction of the solid material ($\sim 5\%$), and this

is reflected in very *soft 'shear' or 'bending' modes* for sound propagating in nematic aerogel. Since the Poisson coefficients for the network structure are negligible ($c_{12} \ll c_{44}$), the matrix of Voigt elastic constants is diagonal to a good approximation,

$$c_{\alpha\beta} = \text{diag}(c_{11}, c_{22}, c_{33}, c_{44}, c_{55}, c_{66}) \\ \approx \text{diag}\left(E\psi\frac{a}{c}, E\psi\frac{a}{c}, E\psi, \frac{3}{2\pi}E\psi^2\frac{a}{c}, \frac{3}{2\pi}E\psi^2\frac{a}{c}, \frac{3}{\pi}E\psi^2\frac{a}{c}\right). \quad (8)$$

In the last line we shall omit the numerical factors on order unity.

III. VIBRATIONAL MODES IN (POLAR) ³HE-NAG

The polar phase is a non-chiral strongly anisotropic superfluid, as follows from its condensate wave function discussed above. It has the maximal superfluid gap oriented along the strands while it vanishes perpendicular to the strands. The densities of both superfluid and normal motions are tensorial quantities assembled into the total density ρ of ³He,

$$\rho\delta_{ij} = \rho_{ij}^n + \rho_{ij}^s, \quad (9)$$

where $\rho_{ij}^{n(s)} = \rho_{\parallel}^{n(s)}\hat{z}_i\hat{z}_j + \rho_{\perp}^{n(s)}\delta_{ij}^{\perp}$, $\delta_{ij}^{\perp} = \delta_{ij} - \hat{z}_i\hat{z}_j$. This structure is strongly reflected in the sound velocities. Near transition temperature (Ginzburg-Landau regime) the anisotropy is large, $\rho_{\parallel}^n/\rho_{\perp}^n \geq 3$. This simply reflects the presence of a nodal line on the gap, the equator of the fermi surface in the plane perpendicular to the strands. There, the quasiparticle excitations (the 'normal' part of the fluid) are easily excited thus suppressing the density of condensate particles near equator. Note that as $T \rightarrow 0$, the excitations would die out i.e. the 'normal' part of the fluid would vanish $\rho_{ij}^n \propto T^2$ and the condensate would become *isotropic* and the 'superfluid' part of density would become equal to the total density. Indeed, $\rho_{ij}^s(T=0) = \rho\delta_{ij}$, Eq. (9), in spite of the gap being anisotropic.

We shall use the set of conservation laws for two-fluid hydrodynamics[13] with density conservation for aerogel ρ_a , ³He ρ , the entropy per unit mass s carried by the normal motion, and the momentum density j_i per unit mass of the ³He-nAG combined system with density tensor for the normal motion $\rho_a\delta_{ij} + \rho_{ij}^n$, and ρ_{ij}^s for the superfluid motion[8, 10, 11],

$$\partial_t\rho_a + \text{div}(\rho_a\mathbf{v}^n) = 0, \partial_t\rho + \text{div}\mathbf{g} = 0, \quad (10)$$

$$\partial_t(\rho s) + \text{div}(\rho s\mathbf{v}^n) = 0, \quad (11)$$

where \mathbf{g} is the momentum density of ³He, $g_i = \rho_{ij}^n v_j^n + \rho_{ij}^s v_j^s$, and $v_j^{n(s)}$ the velocity of the normal (superfluid) motion. The superfluid motion is irrotational, $\text{curl}\mathbf{v}^s =$

0, and its equation of motion is

$$\dot{v}_j^s = -\nabla_j\tilde{\mu}, \quad (12)$$

$$\tilde{\mu} = -s\tilde{T} + \frac{1}{\rho}\tilde{p} + \dots \quad (13)$$

where $\tilde{\mu}$, \tilde{p} , \tilde{T} are the variations of the chemical potential per unit mass, pressure, and temperature in the wave versus equilibrium, ρ the density of ³He in equilibrium. Ellipses mark other possible terms allowed by symmetry [10],[11] that we shall ignore since they are supposed to be small in comparison with the leading terms in (13). The momentum density conservation (second Newton's law) reads

$$\partial_t j_i + \nabla_j \Pi_{ij} = 0, \quad (14)$$

$$j_i = \rho_a v_i^n + g_i = \rho_a v_i^n + \rho_{ij}^n v_j^n + \rho_{ij}^s v_j^s \quad (15)$$

$$\Pi_{ij} = p\delta_{ij} - \sigma_{ij}^R, \quad (16)$$

where the elastic reaction of nAG upon ³He is accounted for by the elastic stress tensor $\sigma_{ij}^R = C_{ijklm}\nabla_l u_m$ where u_m is the strain of the nAG skeleton to which the normal component of ³He is clamped and C_{ijklm} the tensor of elastic constants for nAG. For harmonic motion, when velocities $v^{n(s)}$, and the variations of densities $\tilde{\rho}$, $\tilde{\rho}_a$, entropy \tilde{s} , pressure \tilde{p} , and temperature \tilde{T} in the wave are all proportional to $\exp(i\mathbf{k}\mathbf{r} - i\omega t)$ specified as $\exp ik(z - Ut)$ for a wave propagating in e.g. z -direction with velocity U , $\sigma_{ij}^R = C_{ijklm}\nabla_l\left(\frac{v_m^n}{-i\omega}\right)$.

To find sound velocities, one is solving the above system linearized with respect to $v_j^{n(s)}$, $\tilde{\rho}$, $\tilde{\rho}_a$, \tilde{p} , and \tilde{T} [13]. The parameters below without tilde are those for equilibrium:

$$\partial_t\tilde{\rho} + \rho_{ij}^n\nabla_i v_j^n + \rho_{ij}^s\nabla_i v_j^s = 0, \quad (17)$$

$$s\partial_t\tilde{\rho} + \rho\partial_t\tilde{s} + \rho s \text{div}\mathbf{v}^n = 0, \quad (18)$$

$$\dot{v}_j^s = s\nabla_j\tilde{T} - \frac{1}{\rho}\nabla_j\tilde{p}, \quad (19)$$

$$\rho_a\dot{v}_i^n + \rho_{ij}^n\dot{v}_j^n + \rho_{ij}^s\dot{v}_j^s + \nabla_i\tilde{p} - \nabla_j\left[C_{ijklm}\nabla_l\left(\frac{v_m^n}{-i\omega}\right)\right] = 0, \quad (20)$$

where dot marks the time derivative. A note is in order with regards to Eq. (20): it correctly recovers the limiting cases of sound in a *dry aerogel* where $\rho_{ij}^n = \rho_{ij}^s = 0$, as well as first and (anisotropic) second sound in pure ³He. Thus, the dry nAG shows three sound branches, one longitudinal and two transversal, the latter being degenerate for propagation direction along the growth axis, as expected[12]. Below, we shall drop the effects of (negli-

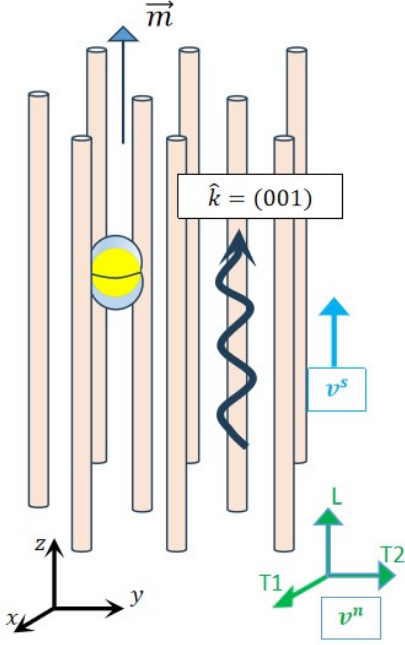


FIG. 2. (Color online) Schematic of sound wave propagating along the strands of nematic aerogel filled with the polar phase of ^3He that shows the Dirac nodal line at the equator plane perpendicular to the nematic director \vec{m} . The irrotational superfluid motion with velocity \mathbf{v}^s follows the wave vector $\hat{k} = (0, 0, 1)$. The normal velocity has one longitudinal and two transversal possible orientations ($L, T1, T2$). The modes $T1$ and $T2$ are degenerate since the nematic aerogel is the transversely isotropic system.

gible) thermal expansion:

$$\tilde{\rho} = \left(\frac{\partial \rho}{\partial p}\right)_T \tilde{p} + \left(\frac{\partial \rho}{\partial T}\right)_p \tilde{T} \approx \left(\frac{\partial \rho}{\partial p}\right)_s \tilde{p} = \frac{\tilde{p}}{u_1^2}, \quad (21)$$

$$u_1^2 \equiv \left(\frac{\partial p}{\partial \rho}\right)_s, \quad (22)$$

$$\tilde{s} = \left(\frac{\partial s}{\partial p}\right)_T \tilde{p} + \left(\frac{\partial s}{\partial T}\right)_p \tilde{T} \approx \frac{c_p}{T} \tilde{T}, \quad (23)$$

where u_1 is the isotropic velocity of first (pressure) sound, c_p the specific heat of ^3He .

A. Sound propagating along the strands with $\hat{k} = (001)$

We start by looking for a longitudinal (L) wave $\mathbf{v}_L^n \propto \hat{z} \exp ik(z-Ut)$ and two degenerate transversal waves (T) $\mathbf{v}_{T1}^n \propto \hat{x} \exp ik(z-Ut)$, $\mathbf{v}_{T2}^n \propto \hat{y} \exp ik(z-Ut)$, where the hats mark unit vectors in a particular direction (choice of x- and y-axes in plane perpendicular to the strands \hat{z} is arbitrary), Fig. 2.

1. L-wave along the strands

The system of linearized equations reads

$$-U\tilde{\rho} + \rho_{\parallel}^n v^n + \rho_{\parallel}^s v^s = 0, \quad (24)$$

$$sU\tilde{\rho} + \rho U\tilde{s} - \rho s v^n = 0, \quad (25)$$

$$Uv^s + s\tilde{T} - \frac{1}{\rho}\tilde{p} = 0, \quad (26)$$

$$\left(\rho_a + \rho_{\parallel}^n\right) Uv^n + \rho_{\parallel}^s Uv^s - \tilde{p} - c_{33} \frac{v^n}{U} = 0. \quad (27)$$

Again, the 'longitudinal densities' $\rho_{\parallel}^{n(s)}$ are involved in dispersion of the waves propagating *along* the strands. Its solution also yields $\tilde{\rho}_a$ through $U\tilde{\rho}_a = \rho_a v^n$. Note that for the longitudinal wave propagating *along the strands* only the densities of ^3He *parallel to the strands* get involved. Using Eqs.(21), (23), this system reduces to a quadratic dispersion equation for the sound velocity U^2 ,

$$\left(U^2 - u_1^2\right) \left(U^2 - u_{2\parallel}^2\right) + \frac{\rho_a}{\rho_{\parallel}^n} \left(U^2 - u_{33}^2\right) \left(U^2 - u_{4\parallel}^2\right) = 0, \quad (28)$$

Here,

$$u_{2\parallel}^2 \equiv \frac{Ts^2}{c_p \rho_{\parallel}^n} \rho_{\parallel}^s, \quad (29)$$

$$u_{4\parallel}^2 \equiv u_1^2 \frac{\rho_{\parallel}^s}{\rho} + \frac{\rho_{\parallel}^n}{\rho} u_2^2, \quad (30)$$

are the (generally anisotropic) second and fourth sound velocities. Above, we have defined $\rho_a u_{33}^2 \equiv c_{33}$, $c_{33} = E\psi = 150 \text{ GPa} \times 0.05 = 7.5 \text{ GPa}$, $\rho_a = \rho_M \psi$ where $\rho_M = 2.80 - 3.1 \text{ g/cc}$ is the density of the bulk (ceramic) mullite, giving the *characteristic* sound velocity in dry nGA $u_{33} \simeq \sqrt{E\psi/(\rho_M \psi)} = 220 \text{ m/s}$ (the solid fraction ψ drops out.) The wave with such large velocity could not be excited in a small nAG sample with linear size about $L = 3 \text{ mm}$. Note that this aerogel mode exists above T_{ca} but is too fast to be excited in 3 mm sample (see below.)

The dispersion equation (28) differs from the one for ^4He in isotropic aerogel[8] by account for anisotropy of both the polar phase and the nematic aerogel. If the aerogel is absent, $\rho_a = 0$, the second term in Eq.(28) vanishes and we recover the Landau equation for the first and (anisotropic in ^3He) second sound, $\left(U^2 - u_1^2\right) \left(U^2 - u_{2\parallel}^2\right) = 0$ [13]. In another limiting case of aerogel mass density $\rho_a \gg \rho_{\parallel}^n$, the second term in (28) dominates, and one recovers the fourth sound in aerogel that acts as a superleak, yet elastic not the rigid one, plus the pressure sound in dry aerogel. The latter is high speed and is hardly relevant for the observations[6].

A short note on *size effect cutoff*: a sound wave with velocity U could be excited at frequency f in a sample with size L provided that $U/(2f) \leq L$ or $U \lesssim U_c \sim 10$

m/s for frequencies $f \lesssim 1600$ Hz [6]. We shall see below that there are (i) slow modes supported by elastic relaxation of the aerogel skeleton that exist above and below transition into the polar phase and (ii) the modes involving the condensate that emerge at T_{ca} with zero velocity that then rises very quickly to the cutoff value U_c , Fig.4. This is likely to be signaled by observed plateau in mechanical resonance of the vibrating wire [5, 6] (see below.)

The general solutions to the quadratic dispersion law (28) for the hybrid second sound U_{2a}^L and the hybrid fourth sound U_{4a}^L are readily found. The remarkable result is that the *hybrid second sound* U_{2a}^L still vanishes at critical temperature T_{ca} of superfluid transition in aerogel in spite of persistent elastic force exerted by aerogel. Near $T = T_{ca}$,

$$\begin{aligned} (U_{2a}^L)^2 &\simeq \tau u_1^2 \frac{\rho_a u_{33}^2 + \rho_{\parallel}^n u_{20}^2}{\rho_a u_{33}^2 + \rho_{\parallel}^n u_1^2} \\ &\approx \tau u_1^2 \frac{\rho_a u_{33}^2}{\rho_a u_{33}^2 + \rho u_1^2}, \end{aligned} \quad (31)$$

$$(U_{4a}^L)^2 \simeq \frac{\rho_n u_1^2 + \rho_a u_{33}^2}{\rho_a + \rho} + C\tau, \quad (32)$$

where $\tau \equiv 1 - T/T_{ca} \ll 1$, $\rho_{\parallel}^n \approx \rho$ (density of ^3He) near T_{ca} , u_{20} the second sound velocity at low temperatures, and C the constant. In the above estimate we accounted for $u_1 \gg u_{20}$ ($u_1 \sim 300$ m/s[11], while $u_{20} \lesssim 3$ cm/s[15]). Note the important *large u_1 factor* in U_{2a} and that it emerges at $T = T_{ca}$, Eq. (31), as $U_{2a} \simeq u_1 \sqrt{\tau}$. This likely relates to the observations where vibrating wire resonant frequency sharply rises upon cooling away from T_{ca} and quickly hits a plateau as a function of temperature caused by the size effect cutoff at $U_{2a}(T) \simeq U_{\text{cutoff}}$. The hybrid fourth sound velocity U_{4a}^L remains finite and large, Eq. (32), see Fig. 4. It cannot be excited in the small mm-size aerogel nAG sample.

2. Transversal waves along the strands, $\hat{\mathbf{k}} = (001)$, $\mathbf{v}^n \perp \hat{z}$, $\mathbf{v}^s \parallel \hat{z}$

In this case the normal velocity $\mathbf{v}^n \propto \{\hat{x}, \hat{y}\} \exp ik(z - Ut)$, normal to the polarization of superfluid velocity that is always pointing along the k -vector, $\mathbf{v}^s \propto \hat{z} \exp ik(z - Ut)$. Compared to the case of sound propagating along the strands (20), the main change is in the dynamics of the momentum density, where superfluid velocity drops out,

$$U(\rho_a + \rho_{\perp}^n) v_x^n - c_{55} \frac{v_x^n}{U} = 0. \quad (33)$$

The dispersion equation for the T-waves reads

$$\left(U^2 - u_{4\parallel}^2\right) \left(U^2 - \frac{\rho_a u_{55}^2}{\rho_a + \rho_{\perp}^n}\right) = 0, \quad (34)$$

where we introduced $\rho_a u_{55}^2 \equiv c_{55} \sim E\psi^2 \frac{a}{c}$, the fourth sound velocity above is

$$u_{4\parallel}^2 = u_1^2 \frac{\rho_{\parallel}^s}{\rho} + u_{2\parallel}^2 \frac{\rho_{\parallel}^n}{\rho}, \quad u_{2\parallel}^2 = \frac{T s^2 \rho_{\parallel}^s}{c_p \rho_{\parallel}^n}. \quad (35)$$

Hence, one gets two degenerate transversal waves with the velocity $U_{55}^T = u_{55} [\rho_a / (\rho_a + \rho_{\perp}^n)]^{1/2}$, and two with the fourth sound velocity $U_{4\parallel}^T = u_{4\parallel}$. Here, we introduced $u_{55} \sim \sqrt{E\psi^2 \frac{a}{c} / \rho_a} = 5$ m/s and the corresponding 'shear' sound velocity near T_{ca} is $U_{55}^T \sim 3$ m/s. This mode is slow enough to be excited in the mm-size aerogel sample. Note that U_{55}^T exist above critical temperature T_{ca} and may be one of the slow modes that Dmitriev *et al.*[5] called the 'main' mode that exists in the normal phase and than experiences an 'avoided' crossing with the additional mode that emerges at T_{ca} , Fig. 4.

Importantly, the *hybrid fourth sound* velocity $U_{4\parallel}^T = u_{4\parallel} \rightarrow 0$ vanishes at T_{ca} in contrast with *hybrid longitudinal fourth* sound velocity which remains finite even at $T = T_{ca}$. One can estimate its behavior near T_{ca} as $U_{4\parallel}^T \sim u_1 \sqrt{\frac{\rho_{\parallel}^s}{\rho}} \sim u_1 \sqrt{0.3\tau}$ in polar phase.

For the latter estimate we have used the results for the superfluid density stemming from the Ginzburg-Landau theory of the polar phase. Namely, $\rho_{\parallel}^s / \rho_{\perp}^s = 3$ in the weak coupling regime, and

$$\frac{\rho_{\perp}^s}{\rho} = \frac{\tau}{\beta_{12345}}, \quad (36)$$

where $\beta_{12345} = \beta_1 + \dots + \beta_5$, are the Ginzburg-Landau parameters. Since the weak coupling approximation is unable to describe the existence of A-phase and other features of ^3He , one would like to use the *strong coupling values* for β_s . For below estimates, we shall use the value $\rho_{\perp}^s / \rho \sim 0.1\tau$ [11].

B. Sound propagating perpendicular to the strands with $\hat{\mathbf{k}} = (1, 0, 0)$

In this case, we again have one longitudinal wave and two transversal waves in dry aerogel and the additional modes due to the global phase coherence of superfluid polar phase of ^3He inside aerogel. In variance with case (A), here the two *transverse waves are not degenerate*. Indeed, for the velocity of normal motion polarizations go like this: L-wave $v^n \parallel x = (v_x^n, 0, 0)$, T1-wave $v^n \parallel z = (0, 0, v_z^n)$, and T2-wave $v^n \parallel y = (0, v_y^n, 0)$, Fig. 3. Since T1-wave would involve the normal density *parallel* to the strands and in the T2-wave one *perpendicular* to the strands, their velocities would be different. Note that the superfluid velocity polarization is parallel to the k -vector and thus perpendicular to the strands, $\mathbf{v}^s \parallel x = (v_x^s, 0, 0)$ in T-waves. To distinguish this case from the previous one for the propagation along the strands, we will mark the resulting velocities by capital S .

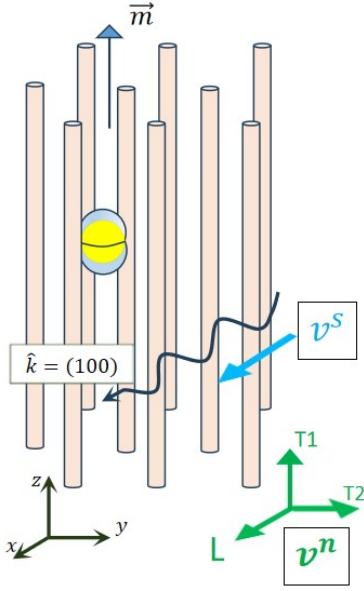


FIG. 3. (Color online) Schematic of sound wave propagating perpendicular to the strands of nematic aerogel filled with the polar phase of ^3He . The superfluid velocity \mathbf{v}^s is collinear with the wave vector $\hat{k} = (1, 0, 0)$. The normal velocity has one longitudinal and two transversal possible orientations ($L, T1, T2$). The modes $T1$ and $T2$ are *not* degenerate: the mode $T1$ involves the normal density along the strands, $T2$ is perpendicular to the strands and they are different reflecting the anisotropy of the superconducting gap.

1. Longitudinal wave propagating perpendicular to the strands

In this case, the normal and superfluid velocities are collinear and oscillate perpendicular to the strands $v^n \parallel x = (v_x^n, 0, 0)$, $v_j^s \parallel x = (v_x^s, 0, 0)$. The momentum density equation for the sound velocity S reads:

$$(\rho_a + \rho_{\perp}^n) S v^n + S \rho_{\perp}^s v^s - \tilde{p} - c_{11} \frac{v^n}{S} = 0. \quad (37)$$

and the full system gives the dispersion equation for L - wave in case $\hat{k} = (1, 0, 0)$

$$(S^2 - u_1^2) (S^2 - u_{2\perp}^2) + \frac{\rho_a}{\rho_{\perp}^n} (S^2 - u_{11}^2) (S^2 - u_{4\perp}^2) = 0, \quad (38)$$

$$u_{2\perp}^2 = \frac{T s^2 \rho_{\perp}^s}{\rho_{\perp}^n c_p}, \quad u_{4\perp}^2 = u_1^2 \frac{\rho_{\perp}^s}{\rho} + u_{2\perp}^2 \frac{\rho_{\perp}^n}{\rho}, \quad (39)$$

where we introduced $\rho_a u_{11}^2 \equiv c_{11} \sim E \psi_c^a$, $u_{11} \simeq 20$ m/s. This yields the hybrid second sound S_{2a}^L and fourth sound S_{4a}^L . The hybrid fourth sound remains finite and large in this case as well, $S_{4a}^L \sim u_1 / \sqrt{2} \simeq 200$ m/s. Near T_{ca} , in full analogy with Eqs. (31),(32),

$$S_{2a}^2 = \tau u_1^2 \frac{\rho_a u_{11}^2}{\rho_a u_{11}^2 + \rho u_1^2}, \quad (40)$$

$$S_{4a}^2 = \frac{\rho_a u_{11}^2 + \rho u_1^2}{\rho_a + \rho}. \quad (41)$$

The hybrid second sound S_{2a} starts at T_{ca} and quickly rises before hitting the linear sample size cutoff, as illustrated by schematic in Fig. 4.

2. Transversal wave propagating perpendicular to the strands (type T1)

Consider the transversal wave with normal velocity polarized along the strands, $v^n \parallel z = (0, 0, v_z^n)$, $v^s \parallel x = (v_x^s, 0, 0)$. The equation for momentum density takes the form,

$$-(\rho_a + \rho_{\parallel}^n) S v_z^n + c_{55} \frac{v_z^n}{S} = 0. \quad (42)$$

The corresponding dispersion equation is for the fourth sound and the 'shear' mode for bending the nematic aerogel in xz -plane (we remind that the x -direction is arbitrary in the plane perpendicular to the strands),

$$(S^2 - u_{4\perp}^2) \left(S^2 - \frac{\rho_a u_{55}^2}{\rho_a + \rho_{\parallel}^n} \right) = 0, \quad (43)$$

where $\rho_a u_{55}^2 = c_{55}$, so that $u_{55} \sim \sqrt{\frac{E \psi_c^a}{\rho_a}} \sim 3$ m/s. Thus, the 'shear' sound $S_{55}^{T1} = u_{55} \sqrt{\frac{\rho_a}{\rho_a + \rho_{\parallel}^n}}$ perpendicular to the strands is really slow on the order of a few m/s. As for the fourth sound, $S_{4\perp}^{T1} = u_{4\perp}$, it emerges at T_{ca} , $S_{4\perp}^{T1} \sim u_1 \sqrt{\rho_{\perp}^s / \rho} \sim u_1 \sqrt{0.1\tau}$, and rises very quickly upon slight cooling from T_{ca} until reaching the size cutoff U_c , similar to the above S_{2a} , Fig. 4.

3. Transversal wave propagating perpendicular to the strands (type T2)

In the last case that we address, $\hat{k} = (100)$, $\hat{v}^n \parallel y$, $\hat{v}^s \parallel k$. The momentum density equation reads

$$(\rho_a + \rho_{\perp}^n) S v_y^n - c_{66} \frac{v_y^n}{S} = 0. \quad (44)$$

and leads to the dispersion equation

$$(S^2 - u_{4\perp}^2) \left(S^2 - \frac{\rho_a u_{66}^2}{\rho_a + \rho_{\perp}^n} \right) = 0, \quad (45)$$

where $\rho_a u_{66}^2 = c_{66} \sim E \psi_c^a$,

$$u_{4\perp}^2 = u_1^2 \frac{\rho_{s\perp}}{\rho} + u_{2\perp}^2 \frac{\rho_{n\perp}}{\rho}, \quad u_{2\perp}^2 = \frac{T s^2 \rho_{s\perp}}{\rho_{n\perp} c_p} \quad (46)$$

and the 'shear' sound in nAG has velocity $S_{66}^{T2} = u_{66} \sqrt{\frac{\rho_a}{\rho_a + \rho_{\perp}^n}} \sim 3$ m/s.

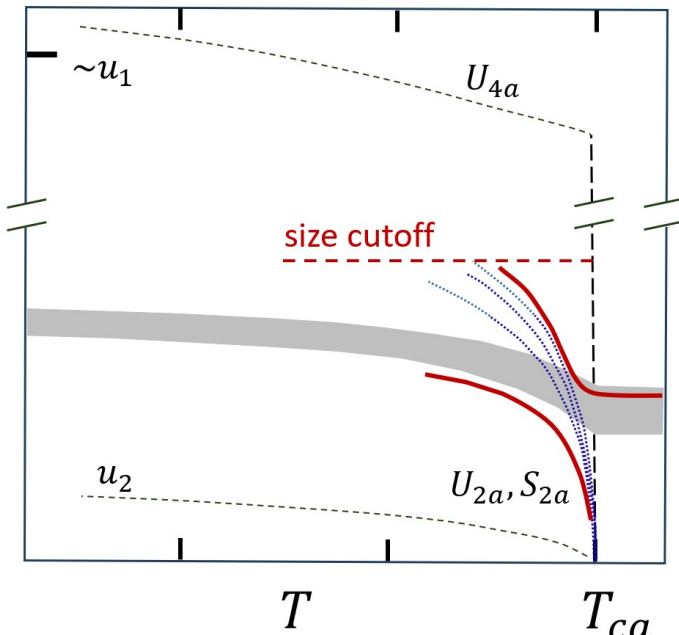


FIG. 4. (Color online) Schematic of the hybrid sound velocities versus temperature in extended nematic aerogel. The hybrid second sound U_{2a} and S_{2a} emerge at the transition into polar phase with zero velocity. Both modes exhibit sharply increasing velocity until they hit the size cutoff that grows linearly with the linear size of aerogel sample (see text.) The shear modes due to elastic response of AG skeleton exist above T_{ca} and weakly depend on temperature (gray band). The observed main VW mode (solid line) exists above T_{ca} and exhibits an avoided crossing with the additional mode that starts at T_{ca} . The velocity of additional mode (upper branch below T_{ca}) increases until it approaches the nAG sample size cutoff corresponding to about 1600 Hz [5].

We see again that the transversal modes for sound propagating perpendicular to the strands of nematic aerogel are very slow, S_{66}^{T2} on the order of a few m/s. Fourth sound for both $T1$ and $T2$ modes, $S_{4\perp}^{T2} = u_{4\perp} \sim u_1 \sqrt{0.1\tau}$, exhibits qualitatively and quantitatively the same behavior. In both cases the fourth sound vanishes at T_{ca} but its velocity increases upon cooling very quickly reaching cutoff limit on the order of 10 m/s signaled by the plateau in frequency dependence of the VW resonance[5], Fig. 4.

The broad overview of the above results is presented in Fig. 4. The main observed mode starts above the transition into the polar phase inside the aerogel sample and continues into the superfluid phase. It is depicted as a gray band since in experiment various modes with different k -vectors get excited giving the main mode a finite width in addition to dissipation. A few additional modes emerge at T_{ca} marked by dashed lines. Those interacting with main mode exhibit avoided crossing as shown on schematic right below T_{ca} . The lower branch is attributed to the main mode below the transition by

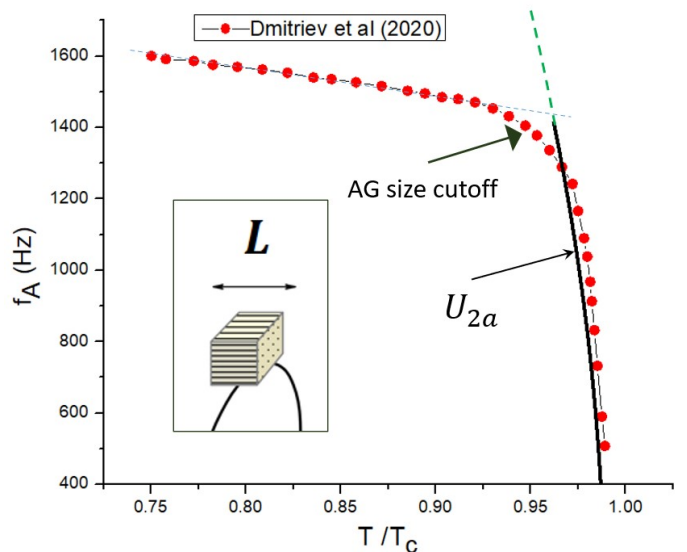


FIG. 5. (Color online) Comparison of the frequency of hybrid second sound U_{2a} with data [5]. The frequency rises sharply from its emergence at T_{ca} . It quickly hits a plateau that is likely due to the velocity of this mode reaching the size cutoff value $U_c \sim 10$ m/s. The size cutoff increases linearly with L (see text). Inset shows the aerogel sample with size $L \approx 3$ mm attached to the vibrating wire [5].

Dmitriev *et al.* and stays at about 450 Hz[5]. The additional mode (the upper branch) exhibits quick increase in velocity before it approaches a finite sample size cutoff.

The hybrid fourth sound U_{4a} is peculiar. It does not go to zero at T_{ca} like in bulk ^3He but retains finite velocity that is on the order of u_1 , the first sound velocity in ^3He . It is too fast to get excited in 3mm aerogel sample. Also shown is the velocity of 'ordinary' second sound u_2 that is very slow indeed compared to the AG modes hybridized with the second sound U_{2a} and S_{2a} , as discussed above, and is not registered either.

The hybrid second sound U_{2a} is compared to the data in Fig. 5. One observes that the model closely follows the data until finite size cutoff is hit signaled by a knee in the data for AG sample with $L = 3$ mm at frequency about 1400 Hz. Incidentally, the cross over for the plateau varies linearly with L and that may potentially be used in future experiments.

IV. DISCUSSION

We have shown above that a simple mechanical model of nematic aerogel yields results for the elastic constants that appear universal since they depend on few generic parameters: AG porosity (the volume fraction of the solid phase $\psi \approx 5\%$), large aspect ratio of connected network of strands $c/a \gg 1$, Fig. 1, and the Young's modulus of the strands' material. This allows building a phenomenological elasto-hydrodynamic- model for the emerging po-

TABLE I. Sound velocities for ^3He in nematic aerogel for different propagation directions and polarizations. The nAG strands are running along $\hat{z}=(001)$ direction.

\hat{k}	\hat{v}^s	\hat{v}^n	U_{2a}^2	U_{4a}^2
(001)	(001)	(001)(L) ^a	$\tau u_1^2 \frac{\rho_a u_{33}^2}{\rho_a u_{33}^2 + \rho u_1^2}$	$\frac{\rho_a u_{33}^2 + \rho u_1^2}{\rho_a + \rho}$
		(100)(T)	$u_{55}^2 \frac{\rho_a}{\rho_a + \rho_{\perp}^n}$	$u_{4\parallel}^2$
		(001)(T) ^b	— —	— —
\hat{k}	\hat{v}^s	\hat{v}^n	S_{2a}^2	S_{4a}^2
(100)	(100)	(100)(L) ^a	$\tau u_1^2 \frac{\rho_a u_{11}^2}{\rho_a u_{11}^2 + \rho u_1^2}$	$\frac{\rho_a u_{11}^2 + \rho u_1^2}{\rho_a + \rho}$
		(001)(T1)	$u_{55}^2 \frac{\rho_a}{\rho_a + \rho_{\parallel}^n}$	$u_{4\perp}^2$
		(010)(T2) ^c	$u_{66}^2 \frac{\rho_a}{\rho_a + \rho_{\perp}^n}$	$u_{4\perp}^2$

^a Values close to T_{ca} , $\tau = 1 - T/T_{ca} \ll 1$. L stands for the longitudinal, T for the transversely polarized sound waves.

^b The transverse velocities are degenerate for the waves propagating along the strands.

^c Superfluid motion is perpendicular to the strands for both T1 and T2 modes resulting in degeneracy of the 4th-like sound velocities.

lar phase of ^3He filling up the nematic aerogel and relate dynamics of sound excitations to the viscous coupling between aerogel strands and the normal motion of ^3He and superfluid backflow. We have found that (i) various slow modes with velocities on the order of few meters per second are excited above and below temperature of transition into the polar phase T_{ca} , reflecting the 'softness' of elastic 'shear' (or 'bending') response by nematic aerogel, (ii) the second sound hybridized with aerogel vibrations starts with zero velocity at T_{ca} . It then exhibits an avoided crossing with the main mode that persists from the normal phase, and quickly hits a cutoff imposed by the finite sample size, see discussion of Fig. 4 in the previous Section. This seems to correlate with observed sharp rise followed by a plateau in resonant frequency of vibrating wire with lowering T [5, 6]. (iii) The fourth sound for waves propagating *perpendicular to the strands*, modes T1 and T2, also vanish at T_{ca} . It is worth noting that the hybrid *longitudinal* fourth sound velocity remains finite irrespective of direction of propagation but is too fast to

be excited in the mm-size aerogel sample. Correspondingly, (iv) there is a size effect cutoff of hybrid second sound irrespective of directions where it propagates and the transversal hybrid fourth sound propagating perpendicular to the strands. All the modes discussed above are classified in the Table.

The current picture offers an alternative view of sound in nematic aerogel studied previously in similar phenomenological models in Refs. [10, 11] yet with large number of free parameters. Here, we have estimated the elastic constants of the aerogel and found analytical solutions for all types of sound in the polar ^3He -nAG not available from prior work. We relate the sharp crossover in observed resonant frequency to the sample size cutoff so that one has no need in assuming a specific fine-tuned weak coupling between e.g. ^3He chemical potential oscillations $\tilde{\mu}$ (13) and axial strain e_3 of the aerogel[11] even though it is allowed by symmetry. More data may shed light onto this interesting interplay.

Obviously, one could not prevent excitation of all modes allowed in aerogel attached to a vibrating wire and their combination should be responsible for the observed resonances. In this regard, experiments with vibrations excited by transducers may be warranted in order to gain more insight into the above-mentioned size effect and other observed features. As far as sharp crossover of resonant frequency with temperature, Fig. 5, the cutoff sound velocity increases linearly with nAG sample size L . This may be another parameter that one may be able to vary within obvious experimental constraints.

We acknowledge many enlightening discussions with V.V. Dmitriev, I.A. Fomin, A.A. Soldatov, E.V. Surovtsev, A.M. Tikhonov, A.M. Troyanovsky, and A.N. Yudin. V.V. Dmitriev, A.A. Soldatov, and A.N. Yudin are gratefully acknowledged for providing samples and sharing data.

V. DATA AVAILABILITY

All data is included in the main text and is available upon reasonable request.

-
- [1] A. J. Leggett, *A theoretical description of the new phases of liquid ^3He* , Rev. Mod. Phys. **47**, 331 (1975).
[2] K. Aoyama and R. Ikeda, *Pairing states of superfluid ^3He in uniaxially anisotropic aerogel*, Phys. Rev. **B 73**, 060504(R) (2006).
[3] V. V. Dmitriev, A. A. Senin, A. A. Soldatov, and A. N. Yudin, *Polar Phase of Superfluid ^3He in Anisotropic Aerogel*, Phys. Rev. Lett. **115**, 165304 (2015)
[4] S. Autti, V. V. Dmitriev, J. T. Mäkinen, A. A. Soldatov, G. E. Volovik, A. N. Yudin, V. V. Zavjalov, and V. B. Eltsov, *Observation of Half-Quantum Vortices in*

Topological Superfluid ^3He , Phys. Rev. Lett. **117**, 255301 (2016).

- [5] V. V. Dmitriev, M. S. Kutuzov, A. A. Soldatov, E. V. Surovtsev, and A. N. Yudin, *Oscillating Nematic Aerogel in Superfluid ^3He* , JETP Lett. **112**, 780 (2020); arXiv:2011.13747.
[6] V.V. Dmitriev, D.V. Petrova, A.A. Soldatov, A.N. Yudin, *Investigations of new phases of superfluid ^3He in nematic aerogel using a vibrating wire*, Phys. Usp. **67**, 1239 (2024), DOI: <https://doi.org/10.3367/UFNe.2024.07.039760>.

- [7] V.V. Dmitriev, M. S. Kutuzov, A. A. Soldatov, and A. N.Yudin, *Superfluid β phase of ^3He* , Phys. Rev. Lett. **127**, 265301 (2021).
- [8] M. J. McKenna, T. Slawacki, and J. D. Maynard, *Observation of a second-sound-like mode in superfluid-filled aerogel*, Phys. Rev. Lett. **66**, 1878 (1991).
- [9] A. Golov, D. A. Geller, and J. M. Parpia, and N. Mulders, *Acoustic Spectroscopy of Superfluid ^3He in Aerogel*, Phys. Rev. Lett. **82**, 3492 (1999); E. Nazaretski, D.M.Lee, and J.M. Parpia, *Superfluid density of ^3He in 98% aerogel in small magnetic fields*, Phys. Rev. B **71** 144506 (2005).
- [10] H. R. Brand and H. Pleiner, *Macroscopic behavior of the distorted A and B phases and the polar phase of superfluid ^3He in an anisotropic aerogel*, Phys. Rev. B **102**, 094510 (2020); *Macroscopic behavior of the $P_1(\beta)$ and P_2 (distorted β) phases of superfluid ^3He : Soundlike excitations*, Phys. Rev. B **105**, 174508 (2022).
- [11] E. V. Surovtsev, *Sound-like Oscillations in the Polar Phase of Superfluid ^3He in a Nematic Aerogel*, JETP Lett. **116**, 745 (2022), DOI: <https://doi.org/10.1134/S0021364022602305>.
- [12] L.D. Landau and E.M. Lifshitz, *Theory of Elasticity* (5th ed., Fizmatlit, 2003).
- [13] L.D. Landau and E.M. Lifshitz, *Hydrodynamics* (6th ed., Fizmatlit, 2021).
- [14] L.J. Gibson and M.F. Ashby, *Cellular Solids* (2nd ed., Cambridge Univ. Press, 1999).
- [15] S. T. Lu and H. Kojima, *Observation of Second Sound in Superfluid ^3He —B*, Phys. Rev. Lett. **55**, 1677 (1985).